ACS Photonics

Article

pubs.acs.org/journal/apchd5

Photoconductive Terahertz Near-Field Detector with a Hybrid Nanoantenna Array Cavity

Oleg Mitrofanov,*[,†,‡] Igal Brener,[‡,§] Ting Shan Luk,[‡,§] and John L. Reno[‡,§]

[†]Electronic and Electrical Engineering, University College London, London, WC1E 7JE U.K.

[‡]Center for Integrated Technologies, Sandia National Laboratory, Albuquerque, New Mexico 87185, United States

[§]Sandia National Laboratory, Albuquerque, New Mexico 87185, United States

Supporting Information

ABSTRACT: Nanoscale structuring of optical materials leads to modification of their properties and can be used for improving efficiencies of photonic devices and for enabling new functionalities. In ultrafast optoelectronic switches for generation and detection of terahertz (THz) radiation, incorporation of nanostructures allows us to overcome inherent limitations of photoconductive materials. We propose and demonstrate a nanostructured photoconductive THz detector for sampling highly localized THz fields, down to the level of $\lambda/150$. The nanostructure that consists of an array of optical nanoantennas and a distributed Bragg reflector forms a hybrid cavity, which traps optical gate pulses within the photoconductive layer. The effect of photon trapping is observed as enhanced absorption at a designed wavelength. This optically thin photoconductive THz detector allows us to detect highly confined evanescent THz fields coupled through a deeply subwavelength aperture as small as 2 μm ($\lambda/150$ at 1 THz). By monolithically integrating the THz detector with apertures ranging from 2 to 5 μm we realize higher spatial resolution and higher sensitivity in aperture-type THz near-field microscopy and THz time-domain spectroscopy.

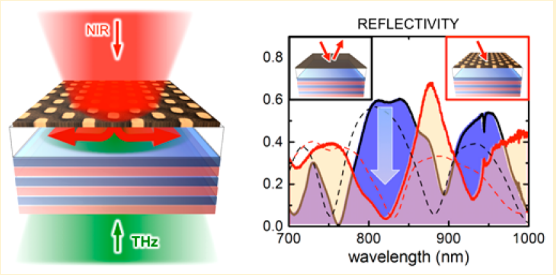

KEYWORDS: *nanoantenna, terahertz, near-field microscopy, light trapping, plasmons*

The use of nanostructures for enhancing optical absorption has enabled optically thin semiconductor photonic devices to be used for a wide range of applications, including high-efficiency, low-cost solar cells[1,2] and photodetectors based on two-dimensional (2D) atomically thin crystals.[3] Nanostructures can also make an impact on the development of photoconductive (PC) terahertz (THz) emitters and detectors.[4−13] A substantial increase in the conversion efficiency has been achieved in PC THz emitters by coupling the photoexcitation to localized plasmonic modes supported by nanostructured electrodes.[5−7] Apart from improving efficiencies, enhancing optical absorption in thin PC layers could enable device concepts deemed impossible until recently. One such device is a PC THz near-field probe for subwavelength resolution THz imaging and spectroscopy[12] in which the input aperture is smaller than $^{1}/_{100}$ of the wavelength. This probe allows mapping the THz electric field distribution in space and time by optically sampling the THz field that couples through the aperture. Spatial resolution of this near-field probe is defined by the aperture size. Applications of this technique with larger apertures have already demonstrated THz imaging and spectroscopy of fundamental modes in subwavelength size THz resonators[14,15] and mapping of THz surface waves[16] and transient photocurrents.[17] Improving the spatial resolution further however entails detection of THz waves transmitted through a single aperture smaller than $\sim \lambda/100$, which so far has been impractical.

In previous work it was shown that incorporation of a THz detector near the input aperture in a monolithic probe enhances its sensitivity.[18−21] This is because the waves transmitted through the subwavelength aperture consist predominantly of evanescent components[22,23] (described by imaginary k-vectors), which cannot be detected by a far-field detector. However, even the monolithic probes have been impractical for PC THz detectors integrated with apertures smaller than 3 μm ($\sim\lambda/100$ at 1 THz). This is due to the fact that the corresponding THz evanescent field region is smaller than the optical absorption length in commonly used PC materials, such as the low-temperature-grown GaAs (LT GaAs). THz detectors based on two-dimensional electron gas (2DEG) in GaAs quantum wells and on an electro-optic crystal were also employed to detect THz fields transmitted through subwavelength apertures.[19,20] The cryogenically cooled ultrathin 2DEG detector[19] in particular can be highly sensitive to the strongly localized evanescent field, and it was demonstrated with apertures as small as 8 μm.[19] However, this detector lacks the capability of coherent (amplitude and phase) and time-resolved detection, presently possible only with optically gated THz detectors.

Received: August 24, 2015
Published: November 19, 2015

DOI: 10.1021/acsphotonics.5b00475
ACS Photonics 2015, 2, 1763−1768

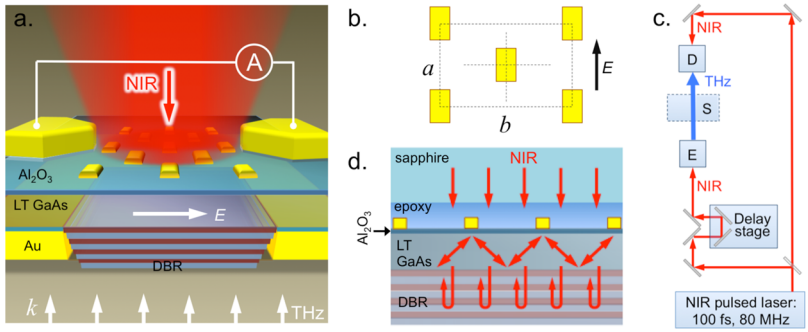

Figure 1. (a) Schematic diagram of the PC THz near-field probe. White arrows indicate the wavevector of the incident THz wave (k) and the electric field (E) induced in the photoconductive region. The red arrow indicates the optical gating pulse (NIR). (b) Unit cell of the antenna array: a = 250 nm, b = 400 nm. The black arrow shows the optical excitation polarization. (c) Schematic diagram of the THz near-field microscopy system with the monolithic PC detector probe: the ZnTe crystal (E) is excited by NIR pulses from the Ti:sapphire laser; the generated THz pulses are directed to the near-field probe (D), where the THz field is sampled by gating the PC THz detector with NIR pulses from the same laser. A sample (S) can be placed between the emitter and the detector for THz near-field imaging and spectroscopy. (d) Schematic cross-section diagram of the photonic structure and its operation principle. The NIR gate pulse (red arrows) is trapped in the LT GaAs layer after scattering on the nanoantenna array shown schematically as yellow squares.

Recent numerical calculations of the evanescent fields near small apertures[12,20] suggested that monolithic PC THz detectors can enable room-temperature time-resolved THz microscopy with apertures smaller than 3 μm if enhanced optical absorption is realized in optically thin (100−300 nm) PC layers. In general, enhanced light absorption has been achieved using the following design principles: (i) light trapping in the absorbing layer by waveguiding,[24−30] (ii) excitation of localized plasmonic modes at the interface with the absorbing layer,[4−10,31,32] and (iii) positioning the thin absorbing layer near a metallic plane (e.g., the Salisbury screen).[33−36] In the monolithic PC THz near-field probe, where the optical gate beam and the THz wave are incident on the detector from opposite directions, a metallic plane would block the THz field. Plasmonic electrodes, on the other hand, may result in an increase of the detector's noise current.[37] Therefore, the most appropriate method to enhance optical absorption for the THz PC detector is to trap the photons in a thin PC region matched in size to the region of localized evanescent THz field.

We propose and demonstrate light trapping in the PC layer using a hybrid optical cavity consisting of a sparse nanoantenna array on one side of the layer and a distributed Bragg reflector (DBR) on the other side. In this structure, the nanoantenna array eliminates the high reflectance at a designated wavelength within the stop band of the DBR almost entirely and traps the optical gate photons by resonant scattering in the optically thin (280 nm) PC layer, now acting also as a waveguide. The photons therefore remain confined in the PC layer until they are absorbed. Enabled by the coupling between the antenna array and the PC layer, this nanostructure provides the possibility for manipulating optical properties of the PC material, enhancing the antenna response within a band substantially narrower than the resonance line width of individual antennas. The photonic structure allows us to maximize the overlap between the THz evanescent field region of the subwavelength aperture and the photoexcitation region as well as to efficiently use the optical gate pulse energy. It enhances responsivity of the subwavelength-aperture THz near-field probe and allows employing 2 μm input apertures, leading to a higher spatial resolution than previously reported.[12]

The structure and the operation principle of the near-field probe are schematically illustrated in Figure 1. The PC detector consists of a 280 nm thick LT GaAs layer with two metallic electrodes separated by a 2 μm wide gap for collecting the photocurrent, a DBR stack made of four pairs of AlAs/$Al_{0.2}Ga_{0.8}As$ layers (thickness of 68 and 58.5 nm, respectively), and a sparse array of gold nanoantennas isolated electrically from the LT GaAs layer by a thin (15−20 nm) layer of Al_2O_3 (Figure 1b). The detector is bonded to a sapphire substrate, which provides optical access to the PC layer. To bring the PC layer as close to the aperture as possible, the DBR stack is etched away everywhere except for a square-shaped area centered between the metallic electrodes. A 300 nm thick metallic screen is deposited on the probe surface around the 466 nm thick DBR stack. As a result, a dielectric-filled aperture is formed in the screen. To prevent short-circuit current in the THz detector, we isolate the metallic screen electrically from the PC layer using a 30 nm thick Al_2O_3 film.

Detection of THz radiation coupled through the aperture is realized in the same manner as with PC THz receivers used in THz time-domain spectroscopy systems. A schematic diagram of the system is shown in Figure 1c. THz pulses are generated in a ZnTe crystal by the process of optical rectification using 100 fs near-infrared (NIR) pulses from a Ti:sapphire laser (λ_o = 820 nm). The THz beam is focused on the aperture area of the probe at normal incidence using a Si lens attached to the ZnTe crystal. The beam size is approximately 500 μm in diameter. The THz field that couples through the aperture induces an oscillating THz electric field in the LT GaAs region (Figure 1a). To detect that field, photoconductivity in the field region is switched on by a NIR gate pulse from the same laser, focused on the PC region through the sapphire substrate using an aspheric lens with NA = 0.5. The photogenerated charge carriers drift in the THz field and produce photocurrent between the electrodes proportional to the instantaneous THz field. The THz pulse waveform is then sampled by varying the arrival time of the gate NIR pulse with respect to the THz pulse using a time-delay stage (Figure 1c).

Within the photonic structure, the gate pulse photons first encounter the array of sparse nanoantennas, which scatter the incident photons.[38−41] The fundamental antenna resonance (along the antenna length) is designed to match the optical excitation wavelength λ_o. Photons scattered into angles larger than the critical angle become trapped in the high-index LT GaAs layer due to total internal reflection (Figure 1d), whereas photons that experience small-angle or no scattering are

DOI: 10.1021/acsphotonics.5b00475
ACS Photonics 2015, 2, 1763−1768

reflected by the DBR stack (Figure 1d). To increase the reflection coefficient of the DBR, the LT GaAs layer thickness itself is chosen to be a multiple of $^1/_4$ of the optical excitation wavelength in GaAs, $L = (1+ {}^1/_4)\lambda_o/n_{GaAs} = 280$ nm.

We design the nanoantenna array to have a plasmonic resonance at the laser excitation wavelength using a commercial finite-difference time-domain (FDTD) solver.[42] The dimensions of each antenna are chosen to be 100 nm × 66 nm × 65 nm (length × width × height) for compatibility with electron beam lithography. When arranged in the configuration shown in Figure 1b and embedded into the dielectric environment shown in Figure 1d, the antenna array without the DBR stack exhibits a broad resonance at 800 nm according to the simulations (see Supporting Information).

First we analyze the optical properties of the photonic structure to evaluate whether it efficiently absorbs NIR photons. The structure without the array shows the characteristic stop-band of a DBR mirror with the center wavelength around 810 nm (Figure 2a,b, black lines). The LT GaAs layer in this case acts as the first high-index layer of the stack, and it absorbs only ∼35% of the incident photons. Combining the DBR with the antenna array however changes the optical properties drastically: the reflectivity spectrum develops a significant drop (from ∼60% to below 5%) within the stop band, similar to that of a dielectric high-index planar cavity. Remarkably, the transmission coefficient at the wavelength of the dip remains practically unchanged.

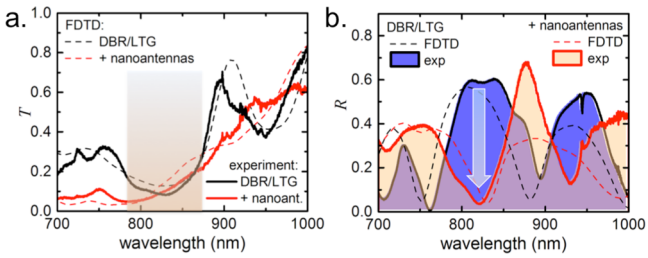

Figure 2. Transmission (a) and reflection (b) spectra of the DBR with the LT GaAs layer (DBR/LTG) with (red) and without (black) the antenna array. Experimental and simulated spectra are shown by the solid and dashed lines, respectively. The shaded area in (a) marks the stop band of the DBR stack; the arrow in (b) indicates the reflectivity drop.

Experimental transmission and reflection are characterized using a linearly polarized, focused broadband optical beam with NA = 0.5, similar to that of the optical gate beam. The experimental spectra closely match the simulated spectra. For the antennas oriented parallel to the beam polarization, the reflection coefficient decreases to 5% at 820 nm, whereas the transmission coefficient remains less than 5% at 800 nm, rising only to 10% at 830 nm. On the basis of the experimental spectra, 80−85% of the NIR gate beam with λ_o in the range 800−830 nm can be absorbed in the photonic structure despite the fact that the LT GaAs layer is thinner than $^1/_4$ of the absorption length. In contrast to the structure without the antenna array, the majority of laser photons are converted into charge carriers in the PC layer. For the probing beam polarized orthogonally to the long axis of the antenna, we find the dip in reflectivity disappears and the transmission spectrum in Figure 2a becomes similar to the spectrum without the antennas.

To understand the origin of this reflectivity dip, we consider the effect of nanoantennas on the field distribution in the LT GaAs layer. The array imposes periodic variation of the optical field in the transverse direction. Therefore, the momentum of photons in the LT GaAs layer has an in-plane component, $k_y = 2\pi/p$, where $p = b = 400$ nm is the array periodicity. The LT GaAs layer therefore can act as a planar waveguide or a cavity with modes described by the total k-vector condition expressed as

$$k_m = \frac{\sqrt{k_y^2 + \frac{\pi^2 m^2}{L^2}}}{n_{GaAs}} \quad (1)$$

where m is an integer.[43] The corresponding wavelength for $m = 2$, $\lambda_2 = 826$ nm, matches the wavelength of the reflectivity dip in Figure 2c. The fact that the spectral width of the reflectivity dip is 50 nm, significantly narrower than the width of the antenna resonance (∼200 nm,; see Supporting Information), confirms that the reflectivity dip corresponds to the hybrid cavity mode, rather than to the pure antenna resonance.

The strong decrease of reflectivity and the lack of a Fabry−Perot peak in the transmission spectrum indicate efficient scattering of the incident photons into the LT GaAs layer. These photons are guided by total internal reflection on one side of the layer and by the DBR stack on the other side until they excite electron−hole pairs. The nanoantenna array therefore transforms the LT GaAs layer into a cavity that traps the incident photons.

The enhancement of optical absorption within the LT GaAs layer is verified by comparing the photocurrent response of identical THz detectors with and without the array (Figure 3a) incorporated into the PC region between the electrodes (Figure 3b). An over 50% increase in the photocurrent is observed for the detectors with nanoantennas. The peak photocurrent, corresponding to the maximum temporal overlap of the THz pulse and the optical gate pulse, reaches ∼500 pA for the gate average power of 5 mW. The photocurrent increase is consistent with the experimentally measured reflectivity and transmission spectra. We emphasize that dark resistance of these detectors remains in the region of 2−3 GΩ after introducing the nanoantennas. The increase in detection

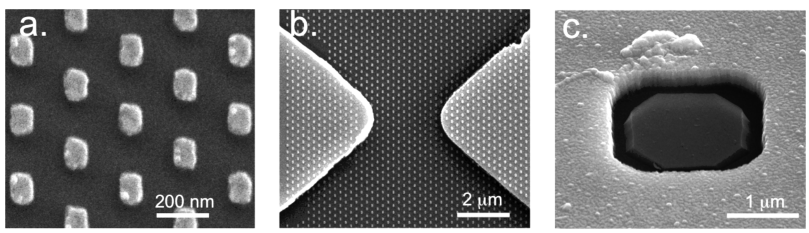

Figure 3. Scanning electron micrographs of the gold antenna array (a); the active region of the THz detector showing two metallic electrodes and the nanoantenna array in the PC gap (b); and a 2 μm square input aperture in the gold screen of the near-field THz probe (c).

DOI: 10.1021/acsphotonics.5b00475
ACS Photonics 2015, 2, 1763−1768

sensitivity therefore is achieved without an increase in detector noise.

The realization of enhanced optical absorption in a thin PC layer allows us to capture the evanescent fields for apertures as small as 2 μm. Waveforms of THz pulses transmitted through square apertures of 2, 3, and 5 μm and their corresponding Fourier spectra are shown in Figure 4a,b. A distinctive THz

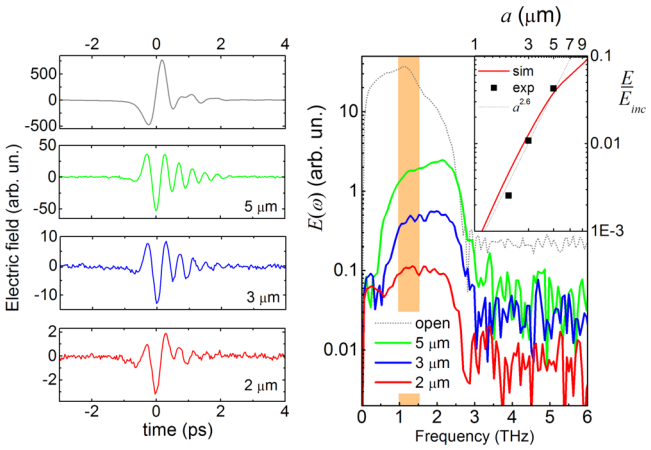

Figure 4. (a) Time-domain waveforms of THz pulses transmitted through the 5, 3, and 2 μm square apertures compared to the incident pulse waveform (top). (b) Fourier transform spectra of the pulses in (a); the inset shows the detected field amplitude as a function of the aperture size; the amplitude is averaged over the 1.0−1.5 THz band (shaded area) and normalized to the corresponding amplitude of the incident pulse.

pulse waveform is detected for all the apertures. The waveform shape agrees with the temporal derivative of the incident pulse waveform.[44] For the 5 μm aperture (λ/60), the detected field amplitude is reduced only by a factor of ∼20, compared to the amplitude of the incident field. This is a significant improvement compared to the factor of ∼1000 found in a monolithic probe employing a 1 μm thick PC layer (without the photonic structure) integrated at 4 μm away from the aperture plane.[18]

For the nanostructured probe, the detected electric field amplitude (averaged in the 1.0−1.5 THz band) follows approximately the $a^{2.6}$ dependence for aperture sizes between 5 and 2 μm (Figure 4b, inset), in agreement with electromagnetic FDTD simulations.[12] Probes with a 2 μm input aperture detect the THz pulse waveform with a practical signal-to-noise ratio. To our knowledge, this is the first demonstration that THz pulses coupled through a 2 μm square aperture (λ/150 at 1 THz) can be detected and used for local THz spectroscopy analysis.

In conclusion, we show that integrating a nanoantenna array and a distributed Bragg reflector with an optically thin PC THz detector enhances optical absorption and results in an increase in detection sensitivity without noise penalty for subwavelength-aperture THz probes. The nanostructured THz PC detector allows us to sense the highly confined THz fields coupled through single apertures as small as 2 μm (λ/150 at 1 THz). The nanostructure provides two critical functions: first of all, it localizes the optical gate pulses uniformly within the evanescent field region of the aperture; second, it efficiently converts the gate pulse photons into photocarriers in an optically thin LT GaAs layer. The concept of a THz near-field probe with an optically thin nanostructured PC THz detector opens doors for improving spatial resolution and sensitivity in subwavelength-aperture THz near-field microscopy. In this work we demonstrate that 2 μm aperture near-field probes (λ/150 at 1 THz) can be employed with full THz time-domain spectroscopy capabilities.

METHODS

The AlAs/$Al_{0.2}Ga_{0.8}As$ DBR stack and the LT GaAs layer are grown by molecular beam epitaxy (wafer number: VB0656) on a semi-insulating GaAs substrate. The substrate temperature is lowered to 250 C during the GaAs layer growth. The samples are subsequently annealed at 600 °C for 40 s. The metallic electrodes are defined lithographically directly on the surface of the annealed samples. The 15−20 nm thick layer of Al_2O_3 is deposited over the whole device using electron beam physical vapor deposition. The nanoantenna array is fabricated by electron beam lithography. Individual THz detectors are cleaved from the wafer and bonded to a 500 μm thick sapphire plate with a transparent nonconductive epoxy (Epotek 353ND). The GaAs substrate is removed using lapping and chemical etching. The exposed DBR stack is then etched away everywhere except for a square-shaped area centered between the metallic electrodes. The insulating Al_2O_3 layer and the 300 nm thick gold screen are deposited instead of the etched DBR layers using electron beam physical vapor deposition. The buried detector electrodes are exposed using chemical etching in an area of the device 5 mm away from the aperture location.

The THz detectors are optically gated by 100 fs pulses from the Ti:sapphire laser with an average power of 5 mW focused to an ∼2−3 μm spot. The photocurrent from the detector is measured by a current preamplifier (DL Instruments) and a lock-in amplifier (Stanford Research Systems, SR830). The typical peak magnitude of the photocurrent in the THz detector with nanoantennas is ∼500 pA for the 5 mW optical excitation power (see Figure 4). Typical variation in detector responsivity (peak photocurrent) for devices in the same fabrication batch is ±10%. No degradation in performance of THz detectors with nanoantennas under the 5 mW optical excitation with typical currents of ∼500 pA has been observed during continuous operation of each detector for 2−3 h/day. Furthermore, no degradation was observed due to prolonged storage of the devices over 3−4 months.

ASSOCIATED CONTENT

Supporting Information

The Supporting Information is available free of charge on the ACS Publications website at DOI: 10.1021/acsphotonics.5b00475.

Supplementary figures showing the resonant response of the nanoantenna array (PDF)

AUTHOR INFORMATION

Corresponding Author

*E-mail: o.mitrofanov@ucl.ac.uk.

Author Contributions

The manuscript was written with contributions of all authors. All authors have given approval to the final version of the manuscript.

Notes

The authors declare no competing financial interest.

DOI: 10.1021/acsphotonics.5b00475
ACS Photonics 2015, 2, 1763−1768

■ ACKNOWLEDGMENTS

This work is supported by the Royal Society (Grant No. UF 130493), and it was performed at UCL and in part at the Center for Integrated Nanotechnologies, an Office of Science User Facility operated for the U.S. Department of Energy (DOE) Office of Science. Sandia National Laboratories is a multiprogram laboratory managed and operated by Sandia Corporation, a wholly owned subsidiary of Lockheed Martin Corporation, for the U.S. Department of Energy's National Nuclear Security Administration under contract DE-AC04-94AL85000.

■ REFERENCES

(1) Atwater, H. A.; Polman, A. Plasmonics for improved photovoltaic devices. *Nat. Mater.* **2010**, *9* (3), 205−213.
(2) Kim, S. J.; Thomann, I.; Park, J.; Kang, J.-H.; Vasudev, A. P.; Brongersma, M. L. Light trapping for solar fuel generation with Mie resonances. *Nano Lett.* **2014**, *14* (3), 1446−1452.
(3) Lei, S.; Wen, F.; Ge, L.; Najmaei, S.; George, A.; Gong, Y.; Gao, W.; Jin, Z.; Li, B.; Lou, J.; Kono, J.; Vajtai, R.; Ajayan, P.; Halas, N. J. An atomically layered InSe avalanche photodetector. *Nano Lett.* **2015**, *15*, 3048−3055.
(4) Jarrahi, M. Advanced Photoconductive Terahertz Optoelectronics Based on Nano-Antennas and Nano-Plasmonic Light Concentrators. *IEEE Trans. Terahertz Sci. Technol.* **2015**, *5* (3), 391−397.
(5) Heshmat, B.; Pahlevaninezhad, H.; Pang, Y.; Masnadi-Shirazi, M.; Lewis, R. B.; Tiedje, T.; Gordon, R.; Darcie, T. E. Nanoplasmonic terahertz photoconductive switch on GaAs. *Nano Lett.* **2012**, *12*, 6255−6259.
(6) Berry, C. W.; Wang, N.; Hashemi, M. R.; Unlu, M.; Jarrahi, M. Significant performance enhancement in photoconductive terahertz optoelectronics by incorporating plasmonic contact electrodes. *Nat. Commun.* **2013**, *4*, 1622.
(7) Tanoto, H.; Teng, J. H.; Wu, Q. Y.; Sun, M.; Chen, Z. N.; Maier, S. A.; Wang, B.; Chum, C. C.; Si, G. Y.; Danner, A. J.; Chua, S. J. Nano-antenna in a photoconductive photomixer for highly efficient continuous wave terahertz emission. *Sci. Rep.* **2013**, *3*, 2824.
(8) Berry, C. W.; Hashemi, M. R.; Jarrahi, M. Generation of high power pulsed terahertz radiation using a plasmonic photoconductive emitter array with logarithmic spiral antennas. *Appl. Phys. Lett.* **2014**, *104* (8), 081122.
(9) Jooshesh, A.; Smith, L.; Masnadi-Shirazi, M.; Bahrami-Yekta, V.; Tiedje, T.; Darcie, T. E.; Gordon, R. Nanoplasmonics enhanced terahertz sources. *Opt. Express* **2014**, *22* (23), 27992−28001.
(10) Jafarlou, S.; Neshat, M.; Safavi-Naeini, S. A hybrid analysis method for plasmonic enhanced terahertz photomixer sources. *Opt. Express* **2013**, *21* (9), 11115−11124.
(11) Peytavit, E.; Lepilliet, S.; Hindle, F.; Coinon, C.; Akalin, T.; Ducournau, G.; Mouret, G.; Lampin, J.-F. Milliwatt-level output power in the sub-terahertz range generated by photomixing in a GaAs photoconductor. *Appl. Phys. Lett.* **2011**, *99*, 223508.
(12) Macfaden, A. J.; Reno, J. L.; Brener, I.; Mitrofanov, O. 3 μm aperture probes for near-field terahertz transmission microscopy. *Appl. Phys. Lett.* **2014**, *104*, 011110.
(13) Ramanandan, G. K. P.; Adam, A. J. L.; Planken, P. C. M. Enhanced terahertz emission from Schottky junctions using plasmonic nanostructures. *ACS Photonics* **2014**, *1*, 1165−1172.
(14) Mitrofanov, O.; Dominec, F.; Kuzel, P.; Reno, J. L.; Brener, I.; Chung, U.-C.; Elissalde, C.; Maglione, M.; Mounaix, P. Near-field probing of Mie resonances in single TiO_2 microspheres at terahertz frequencies. *Opt. Express* **2014**, *22*, 23034−23042.
(15) Khromova, I.; Navarro-Cia, M.; Brener, I.; Reno, J. L.; Ponomarev, A.; Mitrofanov, O. Dipolar resonances in conductive carbon micro-fibers probed by near-field terahertz spectroscopy. *Appl. Phys. Lett.* **2015**, *107*, 021102.
(16) Mueckstein, R.; Mitrofanov, O. Imaging of terahertz surface plasmon waves excited on a gold surface by a focused beam. *Opt. Express* **2011**, *19*, 3212−3217.
(17) Mueckstein, R.; Natrella, M.; Hatem, O.; Freeman, J. R.; Graham, C. S.; Renaud, C. C.; Seeds, A. J.; Linfield, E. H.; Davies, A. G.; Cannard, P. J.; Robertson, M. J.; Moodie, D. G.; Mitrofanov, O. Near-field analysis of terahertz pulse generation from photo-excited charge density gradients. *IEEE Trans. Terahertz Sci. Technol.* **2015**, *5* (2), 260−267.
(18) Mitrofanov, O.; Lee, M.; Hsu, J. W. P.; Pfeiffer, L. N.; West, K. W.; Wynn, J. D.; Federici, J. F. Terahertz pulse propagation through small apertures. *Appl. Phys. Lett.* **2001**, *79*, 907−909.
(19) Kawano, Y.; Ishibashi, K. An on-chip near-field terahertz probe and detector. *Nat. Photonics* **2008**, *2*, 618−621.
(20) Knab, J. R.; Adam, A. J. L.; Shaner, E.; Starmans, H. J. A. J.; Planken, P. C. M. Terahertz near-field spectroscopy of filled subwavelength sized apertures in thin metal films. *Opt. Express* **2013**, *21* (1), 1101−1112.
(21) Misra, M.; Pan, Y.; Williams, C. R.; Maier, S. A.; Andrews, S. R. Characterization of a hollow core fibre-coupled near field terahertz probe. *J. Appl. Phys.* **2013**, *113*, 193104.
(22) Bethe, H. Theory of diffraction by small holes. *Phys. Rev.* **1944**, *66*, 163.
(23) Bouwkamp, C. On Bethe's theory of diffraction by small holes. *J. Philips Res. Rep.* **1950**, *5*, 321−332.
(24) Stuart, H. R.; Hall, D. G. Absorption enhancement in silicon-on-insulator waveguides using metal island films. *Appl. Phys. Lett.* **1996**, *69* (16), 2327−2329.
(25) Yablonovitch, E.; Cody, G. D. Intensity enhancement in textured optical sheets for solar cells. *IEEE Trans. Electron Devices* **1982**, *29* (2), 300−305.
(26) Campbell, P.; Green, M. A. Light trapping properties of pyramidally textured surfaces. *J. Appl. Phys.* **1987**, *62* (1), 243−249.
(27) Panoiu, N. C.; Osgood, R. M. Enhanced optical absorption for photovoltaics via excitation of waveguide and plasmon-polariton modes. *Opt. Lett.* **2008**, *32* (19), 2825−2827.
(28) Catchpole, K. R.; Polman, A. Design principles for particle plasmon enhanced solar cells. *Appl. Phys. Lett.* **2008**, *93*, 191113.
(29) Briscoe, J. L.; Cho, S.-Y. Hybridised extraordinary optical transmission in plasmonic cavity. *Electron. Lett.* **2014**, *50* (24), 1860−1862.
(30) Vasudev, A. P.; Schuller, J. A.; Brongersma, M. L. Nanophotonic light trapping with patterned transparent conductive oxides. *Opt. Express* **2012**, *20* (S3), A385−A394.
(31) Piper, J. R.; Fan, S. Total absorption in a graphene monolayer in the optical regime by critical coupling with a photonic crystal guided resonance. *ACS Photonics* **2014**, *1*, 347−353.
(32) Min, C.; Li, J.; Veronis, G.; Lee, J.-Y.; Fan, S.; Peumans, P. Enhancement of optical absorption in thin-film organic solar cells through the excitation of plasmonic modes in metallic gratings. *Appl. Phys. Lett.* **2010**, *96*, 133302.
(33) Fante, R. L.; Mccormack, M. T. Reflection properties of the Salisbury screen. *IEEE Trans. Antennas Propag.* **1988**, *36* (10), 1443−1454.
(34) Thareja, V.; Kang, J.-H.; Yuan, H.; Milaninia, K. M.; Hwang, H. Y.; Cui, Y.; Kik, P. G.; Brongersma, M. L. Electrically tunable coherent optical absorption in graphene with ion gel. *Nano Lett.* **2015**, *15* (3), 1570−1576.
(35) Kats, M. A.; Blanchard, R.; Genevet, P.; Capasso, F. Nanometre optical coatings based on strong interference effects in highly absorbing media. *Nat. Mater.* **2013**, *12*, 20−24.
(36) Park, J.; Kang, J. H.; Vasudev, A. P.; Schoen, D. T.; Kim, H.; Hasman, E.; Brongersma, M. L. Omnidirectional Near-Unity Absorption in an Ultrathin Planar Semiconductor Layer on a Metal Substrate. *ACS Photonics* **2014**, *1* (9), 812−821.
(37) Wang, N.; Jarrahi, M. Noise analysis of photoconductive terahertz detectors. *J. Infrared, Millimeter, Terahertz Waves* **2014**, *34*, 519−528.

DOI: 10.1021/acsphotonics.5b00475
ACS Photonics 2015, 2, 1763−1768

(38) Rosenblatt, D.; Sharon, A.; Friesem, A. Resonant grating waveguide structures. *IEEE J. Quantum Electron.* **1997**, *33*, 2038−2059.
(39) Fevrier, M.; Gogol, P.; Aassime, A.; Mégy, R.; Delacour, C.; Chelnokov, A.; Apuzzo, A.; Blaize, S.; Lourtioz, J.-M.; Dagens, B. Giant coupling effect between metal nanoparticle chain and optical waveguide. *Nano Lett.* **2012**, *12*, 1032−1037.
(40) Arango, F. B.; Kwadrin, A.; Koenderink, A. F. Plasmonic antennas hybridized with dielectric waveguides. *ACS Nano* **2012**, *6* (11), 10156−10167.
(41) Schwarz, I.; Harats, M. G.; Livneh, N.; Yochelis, S.; Strauss, A.; Zimran, A.; Banin, U.; Paltiel, Y.; Rapaport, R. Theory and experiments of Bragg cavity modes in passive and active metallic nanoslit array devices. *J. Opt. Soc. Am. B* **2012**, *29* (2), A127−A137.
(42) See http://www.lumerical.com/tcad-products/fdtd/ for Lumerical Solutions, Inc., Lumerical FDTD Solutions.
(43) Novotny, L.; Hecht, B. *Principles of Nano-Optics*; Cambridge University Press, 2012
(44) Mitrofanov, O.; Pfeiffer, L. N.; West, K. W. Generation of low-frequency components due to phase-amplitude modulation of subcycle far-infrared pulses in near-field diffraction. *Appl. Phys. Lett.* **2002**, *81*, 1579−1581.

DOI: 10.1021/acsphotonics.5b00475
ACS Photonics 2015, 2, 1763−1768